Absence of fractal quantum criticality in the quantum Newman-Moore model

Raymond Wiedmann,[1,2] Lea Lenke ®,[1] Matthias Mühlhauser,[1] and Kai Phillip Schmidt ®[1]

[1]*Department of Physics, Staudtstraße 7, Friedrich-Alexander-Universität Erlangen-Nürnberg (FAU), 91058 Erlangen, Germany*
[2]*Max-Planck-Institut für Festkörperforschung, Heisenbergstraße 1, 70569 Stuttgart, Germany*

The quantum phase transition between the low-field fracton phase with type-II fracton excitations and the high-field polarized phase is investigated in the two-dimensional self-dual quantum Newman-Moore model. We apply perturbative and numerical linked-cluster expansions to calculate the ground-state energy per site in the thermodynamic limit, revealing a level crossing at the self-dual point. In addition, high-order series expansions of the relevant low-energy gaps are determined using perturbative continuous unitary transformations indicating no gap closing. Our results therefore predict a first-order phase transition between the low-field fracton and the high-field polarized phase at the self-dual point.

I. INTRODUCTION

Fracton phases of matter are connected to intriguing phenomena such as topological order, glassy dynamics, and spin liquids [1]. Due to this and their potential applications in quantum memories [2], there has been increasing interest in models exhibiting such phases in the last years [3–6]. One of the most important properties of systems with fracton order is the restricted mobility of their low-energy elementary excitations, dubbed fractons [1], which can be of type I or II. In type-I fracton phases, topologically nontrivial composites of the low-energy excitations are still mobile on the lattice, but usually restricted to lower dimensions (submanifolds), i.e., in three dimensions (3D) they can only move on planes or along lines [7]. In contrast, type-II fractons are fully immobile on the lattice.

Well-known examples for models exhibiting fracton properties in 3D are the X-cube model, as introduced in Ref. [7], with type-I fractons, and Haah's code [8] as an example for a type-II fracton order. The quantum robustness of the fracton order in these systems has been studied using quantum Monte Carlo simulations [9] and perturbative linked-cluster expansions [10]. It is found that in both models the fracton phase breaks down by a first-order quantum phase transition when applying an external field. The same behavior is found when studying the competition of fracton order in the X-cube model and intrinsic topological order in the three-dimensional toric code [11]. The occurrence of only first-order transitions can be traced back to the (partial) immobility of the fractons since the low-energy excitations cannot lower their energy sufficiently by quantum fluctuations to induce a second-order phase transition.

Fascinatingly, the two-dimensional (2D) quantum version of the Newman-Moore model [12], exhibiting type-II

fracton order, has been recently suggested to display a continuous quantum phase transition with an exotic fractal criticality based on quantum Monte Carlo simulations and field-theoretic arguments [13]. Here, the low-energy quantum dynamics in the low-field fracton phase is intimately linked to 2D fractal structures of Sierpinksi triangles giving rise to glassy dynamics at finite temperature in the classical Newman-Moore model. Furthermore, the quantum Newman-Moore model (qNM) features an exact self-duality relating the energy spectra of the low-field fracton and the high-field polarized phase. The zero-temperature phase transition between these phases is therefore located at the self-dual point [13,14]. However, the quantum Monte Carlo simulation performed in Ref. [13] is challenging due to the glassy dynamics as well as finite-size effects, and in addition, earlier numerical calculations in Ref. [14] based on transition path sampling indicate a first-order transition. In this work, we clarify this situation by applying perturbative and numerical linked-cluster expansions to investigate this phase transition directly in the thermodynamic limit and at zero temperature. Our results for the ground-state energy and the relevant low-energy excitation energies predict a first-order phase transition between the low-field fracton and the high-field polarized phase at the self-dual point in the qNM.

II. QUANTUM NEWMAN-MOORE MODEL

The qNM is the spin-1/2 Newman-Moore model [12] in a transverse field,

$$\mathcal{H}_{\mathrm{qNM}} = -J \sum_{\triangledown} \sigma_i^z \sigma_j^z \sigma_k^z - \Gamma \sum_i \sigma_i^x. \qquad (1)$$

Here, the sum over $\triangledown$ (i) runs over the downward-pointing triangles (sites) of a triangular lattice as illustrated in Fig. 1. The first term of the Hamiltonian is a three-spin Ising interaction with $J > 0$ acting only on downward-pointing triangles $\triangledown$, while the second term is the transverse magnetic field with field strength $\Gamma > 0$. We note that the number of sites N is equal to the number of downward-pointing triangles.
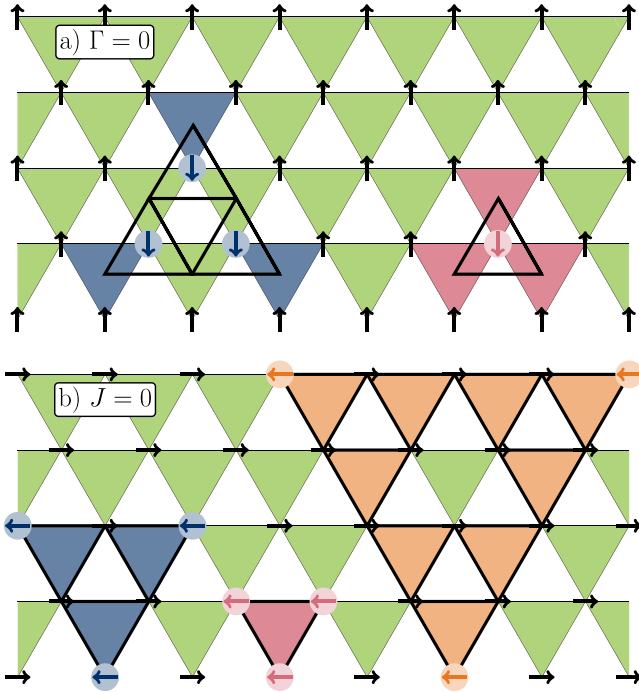
FIG. 1. Low-field limit $\Gamma = 0$ [high-field limit $J = 0$] of the qNM on the triangular lattice with spins-1/2 indicated as black arrows and three-spin interactions acting on downward-pointing triangles ∇ is illustrated in (a) [in (b)]. (a) In the low-field limit $\Gamma = 0$ the fully polarized state with spins pointing in the z direction is one ground state, so that all pseudospins on the centers of downward-pointing triangles point also upward. A single spin-flip changes the eigenvalue of the three attached pseudo-spins on downward-pointing triangles, which is illustrated in red. The three-spin-flip excitation on the next larger Sierpinski triangle is shown in blue. (b) In the high-field limit $J = 0$ the fully polarized state with spins pointing in the x direction is the unique ground state. Fully mobile excitations in the high-field limit are associated with flipping the three spins on a downward-pointing triangle (shown in red) as well as on the first and second nontrivial Sierpinski triangle illustrated in blue and orange, respectively.

Each three-spin Ising interaction has eigenvalues ± 1. One can therefore introduce a pseudo-spin-1/2 τ_μ at the center μ of each ∇ so that $-J \sum_\mu \tau_\mu^x$ yields the correct energy of the three-spin Ising interactions. The local field operator σ_i^x flips the eigenvalues of the three Ising interactions (pseudo-spins) containing site i so that the dual qNM reads

$$\mathcal{H}_{\text{qNM}}^{\text{dual}} = -J \sum_\mu \tau_\mu^x - \Gamma \sum_{\triangle_{\text{dual}}} \tau_\mu^z \tau_\nu^z \tau_\kappa^z, \qquad (2)$$

which is defined on the triangular lattice formed by the centers μ of each ∇ [see Fig. 1(a)]. The qNM is therefore self-dual and the energy spectra of the low- and high-field phase are isospectral. Consistently, the quantum phase transition is found at the self-dual point $J = \Gamma$ [13,14].

The self-duality does not hold for degeneracies and states. In the low-field phase $\Gamma < J$, the qNM displays type-II fracton order. For the limiting case $\Gamma = 0$ ground states have all eigenvalues of three-spin interactions $+1$. This is either realized when all spins point in the positive z direction

[see Fig. 1(a)] or when two of the three spins per triangle are flipped. Therefore, the ground-state manifold is highly degenerate. Within the fracton phase $0 < \Gamma < J$, one finds that the degeneracy scales subextensively with N [13], which is one hallmark of fracton order. In contrast, in the high-field phase with $\Gamma > J$, the qNM is in a featureless polarized phase with a nondegenerate ground state. For $J = 0$ this ground state is the product state where all spins point in the positive x direction [see Fig. 1(b)].

Elementary quasiparticle (QP) excitations in the high-field phase correspond to dressed spin-flip excitations, while the elementary fracton excitation in the low-field phase is related to a negative eigenvalue of a three-spin Ising interaction which becomes dressed at finite fields (see Fig. 1 for both phases). Due to the self-duality, it is sufficient to determine the energetic properties of the trivial high-field phase. The associated energies in the low-field fracton phase can be deduced directly by interchanging J and Γ.

III. LINKED-CLUSTER EXPANSIONS

We use a variant of linked-cluster expansions [15,16] designed for multispin interactions as perturbation [17] to calculate the ground-state energy per site and relevant excitation energies of the high-field polarized phase in the thermodynamic limit. For this phase the three-spin interactions always link the three sites of a ∇. One therefore performs a full graph decomposition in terms of connected ∇s. The calculation on the linked, i.e., possibly contributing, graphs can be done either perturbatively or numerically using exact diagonalization. After embedding all graph contributions into the thermodynamic limit, one then obtains either a high-order series expansion in J/Γ or a numerical data sequence for fixed ratio J/Γ. While the perturbative linked-cluster expansion is exact up to the calculated perturbative order, the numerical linked-cluster expansion (NLCE) [18] includes all quantum fluctuations in the thermodynamic limit up to the length scale set by the maximally extended graph. We refer to Appendix A for technical details about linked-cluster expansions.

Concretely, for the ground-state energy per site $E_0/(\Gamma N)$, we apply perturbative and numerical linked-cluster expansions. We consider all 186 061 nonisomorphic connected clusters from 1 to 13 triangles. This allows us to calculate the perturbative series of $E_0/(\Gamma N)$ up to order 26 in J/Γ in the thermodynamic limit using matrix perturbation theory [16]. Here, the perturbation always has to act on each ∇ an even number of times so that graphs up to 13 triangles are sufficient in order 26 and only even orders contribute in the series expansion. Within the NLCE we define the term order to be twice the maximal number of triangles of the involved clusters, which again yields a maximal order of 26.

To derive high-order series expansions of relevant excitation gaps in the high-field phase, we use perturbative continuous unitary transformations (pCUTs) [19,20] (see also Appendix A). The pCUT method maps Hamiltonian (1) perturbatively in J/Γ to an effective Hamiltonian, which conserves the number of (dressed) spin-flip excitations corresponding to the elementary QP of the high-field phase. The effective Hamilton is therefore block diagonal and each QP block can be treated separately. In this work we calculated the

low-energy excitation gaps of the 1QP, 2QP, and 3QP sector. The explicit series are listed in Appendix B.

Due to the exact self-duality of the qNM, the energetic properties of the QP are identical to the fracton excitations in the low-field phase. As a consequence, individual QPs are strictly local while pairs of QPs are always only linked to a finite number of 2QP configurations so that one is left with diagonalizing finite matrices in the 2QP sector. We denote the lowest excitation gaps in the 1QP and 2QP sector by Δ_1 and Δ_2, which we have calculated perturbatively up to order 14 and 12 in J/Γ, respectively. The 3QP sector contains low-energy excitations which are fully mobile. Indeed, considering three spin flips on the same $\triangledown$, this configuration can either hop to other $\triangledown$ or can be deformed to other 3QP configurations where the three spin-flips are located at the corners of Sierpinski triangles of arbitrary size. These 3QP configurations on Sierpinski triangles can again hop. In the calculated perturbation order 12 this part of the 3QP sector contains three different types of Sierpinski triangle 3QP configurations with side length one, two, and four [see Fig. 1(b)]. Exploiting translational invariance, this infinitely large sector can then be reduced to a 3×3 matrix for fixed momentum. We find that the energy gap in the 3QP sector is located at zero momentum and we denote the three eigenvalues as $\Delta_3^{(n)}$ with $n \in \{1, 2, 3\}$. The $\Delta_3^{(n)}$ can then be extracted as series expansions in order 12 by diagonalizing the 3×3-matrix order by order.

For our analysis, we can extract information about the behavior of the system directly from the bare perturbative and numerical series and, additionally, from extrapolations of the perturbative series which can increase the radius of convergence and give access to potential critical exponents. Here, we use Dlog Padé extrapolation techniques, which are described in Appendix C. This includes biased Dlog Padé extrapolations, where we incorporate that the phase transition takes place at the self-dual point $J = \Gamma$.

IV. GROUND-STATE ENERGY

Results for the ground-state energy per site $E_0/(\Gamma N)$ are shown for both phases in Fig. 2. All displayed results are well behaved and well converged. The low- and high-field energies intersect by construction exactly at the self-dual point $J/\Gamma = 1$ with a clearly visible kink. This kink can be quantified by the angle

$$\beta = \left(\lim_{J/\Gamma \downarrow 1} - \lim_{J/\Gamma \uparrow 1} \right) \left| \arctan \left(\frac{\partial}{\partial (J/\Gamma)} \frac{E_0}{\Gamma N} \right) \right|, \quad (3)$$

which is shown in the right inset of Fig. 2 as a function of 1/order using the perturbative or numerical linked-cluster expansions. One finds that both agree in high orders yielding a finite angle $\beta \approx 15°$ in the infinite-order limit. A rough lower bound for the angle at infinite order can be obtained by performing a linear fit for the three values of highest order, resulting in $\beta \approx 15.23(1)°$ [$\beta \approx 15.19(3)°$] for the perturbative [numerical] data sequence. This finite angle corresponding to the presence of a kink in the ground-state energy at the self-dual point is quantitative evidence that the quantum phase transition in the qNM between the low-field fracton phase and the high-field polarized phase is first order.
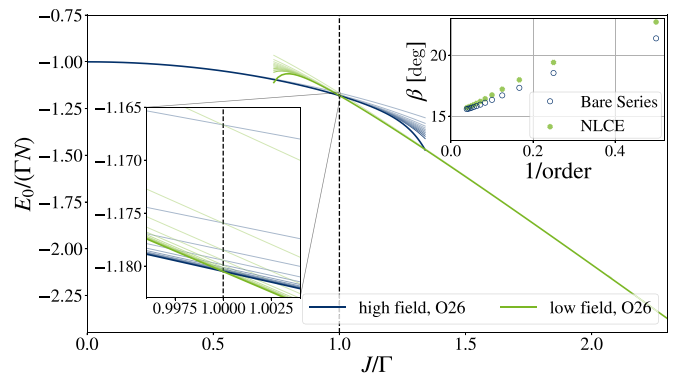

FIG. 2. Series expansion of the ground-state energy per site $E_0/(\Gamma N)$ up to order 26 in J/Γ for the low- and high-field phase. The individual orders of the series are shown with increasing opacity. The highest order is further highlighted in bold as indicated in the legend. By construction, the series intersect in all orders at the self-dual point $J/\Gamma = 1$ marked by the vertical dashed line (left inset zoom close to the self-dual point). Note that the energies from numerical linked cluster expansions are in quantitative agreement with the ones from the series expansions on the displayed energy resolution. The right inset shows the angle β between the low- and high-field energy expression from the perturbative (empty circles) and numerical linked-cluster expansions (filled circles) as a function of 1/order.

Next, we check the reliability of these considerations by applying DLog Padé approximation to the perturbative series of the second derivative of $E_0/(\Gamma N)$ with respect to J/Γ. We bias the DLog Padé approximation to have a pole at the self-dual point $J/\Gamma = 1$. This allows then to extract the critical exponent α. A first-order phase transition implies $\alpha = 0$. Our results for the critical exponent α are shown in Fig. 3, which are again well converged for the high-order DLog Padé approximants. We obtain a critical exponent of $\alpha_{\text{bias}} \approx 0.007(12)$, taking the average of the highest order value for every family. This finding is obviously fully consistent with a first-order phase transition. Note that this is in contradiction to the scenario of fractal quantum criticality
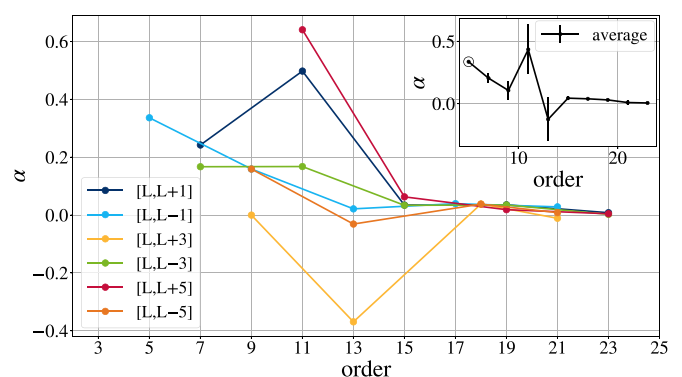
FIG. 3. Critical exponent α from various biased DLog Padé approximants of the second derivative of $E_0/(\Gamma N)$ with respect to J/Γ displayed as a function of the order of the DLog Padé approximant. The results are grouped in families ([L,L+C] with order 2L+C) and shown for $|C| \leqslant 5$. The inset plot shows the average value for each order with the sample standard deviation. For the lowest-order value only a single value is available, marked by a circle.

proposed in Ref. [13] but in accordance with the numerical findings by Vasiloiu *et al.* [14].

V. EXCITATIONS GAPS

Our analysis of the ground-state energy revealed a first-order phase transition at the self-dual point $J/\Gamma = 1$. As a consequence, one expects that all low-energy excitation energies of the high-field phase remain finite for $J/\Gamma \leqslant 1$. This we investigate next by analyzing the series of low-energy excitation energies in the 1QP, 2QP, and 3QP sector. Due to the restricted mobility of single and pairs of QP excitations, we do not expect the associated gaps in these sectors to close. Indeed, a single QP, corresponding to a dressed spin-flip excitation in the high-field phase (or equivalently to a dressed elementary fracton excitation in the low-field phase), is strictly local and has no finite dispersion. It can nevertheless reduce its energy by local fluctuations induced by the three-spin Ising interactions. The same is true in the 2QP sector. If the two QPs are far apart from each other, the QPs are not able to hop in a given perturbative order so that the 2QP continuum is flat in momentum space with twice the energy of a single QP. Only certain 2QP configurations are connected to a finite number of other 2QP configurations if the QPs are sufficiently close. This leads to 2QP energies below the 2QP continuum but not to a finite dispersion. In contrast, the 3QP sector is the first low-energy sector which contains fully mobile excitations. Considering three spin flips on a $\triangledown$, this bound 3QP object can move to other triangles starting in order two perturbation theory, leading to a finite dispersion. At the same time, the bound object on a $\triangledown$ can be deformed into 3QP configurations where the three QPs are located on the corners of a Sierpinski triangle. For the first five nontrivial Sierpinski triangles $\{\triangledown_2, \triangledown_3, \triangledown_4, \triangledown_5, \triangledown_6\}$ the order of perturbation needed to obtain it from the Sierpinski triangle before ($\triangledown_{n-1}$) is given by $\{\triangledown_2 : 2, \triangledown_3 : 6, \triangledown_4 : 18, \triangledown_5 : 54, \triangledown_6 : 162\}$, i.e., the order always increases by a factor of three. The resulting low-energy excitations in the 3QP sector are therefore dispersive and superpositions of Sierpinski triangle 3QP configurations. As a consequence, one therefore expects quantum fluctuations to be most important in the 3QP sector.

In Fig. 4, we show averaged DLog Padé approximations of the 1QP and 2QP gaps Δ_1 and Δ_2 as well as the two lowest excitation energies $\Delta_3^{(1)}$ and $\Delta_3^{(2)}$ with zero momentum in the 3QP sector. Note that DLog Padé approximants with poles at values $J/\Gamma < 1$ are excluded in the averages. Not surprisingly, standard deviations increase for all excitation energies when approaching the self-dual point $J/\Gamma = 1$. Nevertheless, they are small enough to conclude the absence of a gap closing in all three QP sectors, which further confirms the presence of a first-order phase transition.

VI. CONCLUSIONS

In this work we applied perturbative and numerical linked-cluster expansions to investigate the quantum phase transition in the qNM. Our results for the ground-state energy revealed the presence of a finite kink at the self-dual point $J/\Gamma = 1$. This finding is further consistent with the analysis of the second derivative of the ground-state energy as well as with the
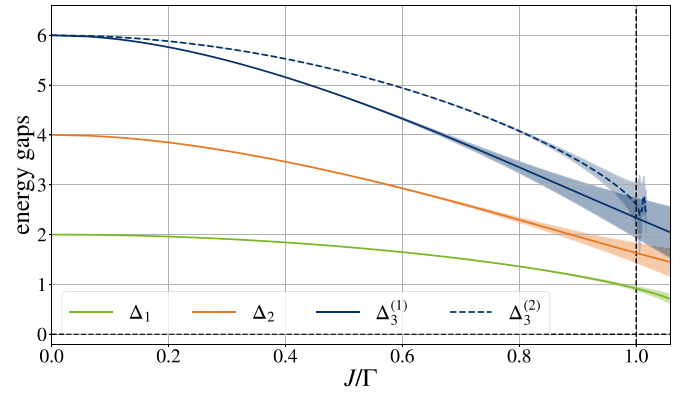
FIG. 4. Low-energy excitation gaps Δ_1 of the 1QP, Δ_2 of the 2QP, and $\Delta_3^{(1)}$ and $\Delta_3^{(2)}$ of the 3QP sector are shown as a function of J/Γ using average and standard deviation of nondefective DLog Padé approximants. The vertical dashed line indicates the self-dual point.

absence of any gap closing in the 1QP, 2QP, and 3QP sector. Our results therefore demonstrate the presence of a first-order phase transition in the qNM, which is in contradiction to the scenario of fractal quantum criticality proposed in Ref. [13]. In particular, their critical value $\alpha = 0.28(2)$ is not consistent with our finding $\alpha_{\text{bias}} = 0.007(12)$. One might speculate that the results in Ref. [13] from quantum Monte Carlo simulations suffer from finite-size effects or from the glassy dynamics present at finite temperatures. Indeed, in Ref. [21] it has been shown that boundary conditions and finite-size effects are nontrivial in the qNM and that the approach to the thermodynamic limit is different across different system sizes and geometries. This is different in our approach using linked-cluster expansions, which have the benefit to work directly in the thermodynamic limit, only truncating in the length scale of the treated quantum fluctuations. Furthermore, our results are in accordance with the numerical results by Vasiloiu *et al.* [14], who also found a first-order transition in the qNM. Another attractive route for a better understanding of the qNM are experimental investigations which have been proposed for Rydberg atom arrays in Ref. [22].

APPENDIX

The Appendix contains three parts. First, we describe the most essential aspects of perturbative and numerical linked-cluster expansions used in this work. Second, we list the bare series of the ground-state energy per site as well as the low-energy excitation gaps. Third, we briefly describe Dlog Padé extrapolations.

APPENDIX A: LINKED-CLUSTER EXPANSIONS

General introductions to linked-cluster expansions can be found in the literature [15,16]. Further, the variant used in this work for multispin interactions as perturbation is detailed in Ref. [17]. In the following we discuss the most important aspects of linked-cluster expansions relevant to this work. First, we consider a Hamiltonian defined on a lattice $\mathcal{L}$,

$$H = \sum_{i \in \mathcal{L}} H_{0,i} + \sum_b V_b, \tag{A1}$$

where the first sum runs over all sites and the second one over the bonds (which are sets of sites in this case). The strictly local $H_{0,i}$ are equivalent for all sites i, and similarly the perturbation terms V_b are equivalent for any bond b. In $\mathcal{H}_{\mathrm{qNM}}$ the sites i host the spin degrees of freedom and the bonds are the $\triangledown$ consisting of three sites. Furthermore, for simplicity, we assume that each $H_{0,i}$ has a unique ground state $|0\rangle$ and a unique excited state $|1\rangle$.

For the ground-state energy and low-energy excitation gaps it is possible to obtain perturbative series expansions which are valid in the thermodynamic limit up to any finite perturbation order from calculations on appropriately designed finite clusters. For the extensive ground-state energy, this is a direct consequence of the linked-cluster theorem which has been generalized to single- and multiparticle excitation energies [19,20,23–25]. As a consequence all matrix elements necessary to calculate the ground-state energy and low-energy excitation gaps can be determined on a finite cluster C.

The idea behind linked-cluster expansions is to decompose the calculation of such a matrix element on a cluster C as [15]

$$K(C) = \sum_{c \subseteq C} \kappa(c), \tag{A2}$$

where the sum runs over all connected subclusters of C and $\kappa(c)$ is the reduced contribution of the cluster c. Note that we mean all connected subclusters of C, not structurally distinct ones. From Eq. (A2) one finds that the reduced contribution of a cluster C is given as

$$\kappa(C) = K(C) - \sum_{c \subset C} \kappa(c), \tag{A3}$$

where the reduced contributions of all proper subclusters of C are subtracted from $K(C)$. Hence, only the part of $K(C)$ coming from the entire cluster C is kept in the reduced contribution. A key element of linked-cluster expansions is to identify structurally equivalent clusters as Hamiltonians (resulting from the restriction of H) on structurally equivalent clusters are the same up to a renumbering of the sites [15]. Accordingly, one can identify equivalent matrix elements of the respective effective Hamiltonians and the sum in Eq. (A2) can be rewritten as [15,16]

$$K(C) = \sum_{g \subseteq C} N(g, C) \kappa(g), \tag{A4}$$

where g is an equivalence class of clusters and the embedding factor $N(g, C)$ is the number of subclusters in the lattice which belong to this class. The sum runs over all classes of connected subclusters of C. The clusters are assigned to classes based on their structure and the product states considered in the matrix element $K(C)$, such that the contributions of the clusters in a class g correspond to equivalent matrix elements

$$\kappa(c) = \kappa(g) \quad \forall \, c \in g. \tag{A5}$$

As $\kappa(g)$ is the same for any cluster in g, it is sufficient to evaluate it once on a representative cluster for any relevant class g. If $N(g, C)$ is extensively large it is normalized to some suitable unit of the lattice [15,16]. In this work we calculated the ground-state energy per bond, normalizing $N(g, C)$ to the number of bonds. Consequently, also the reduced contribution can be written in terms of these classes [15,16]:

$$\kappa(g) = K(g) - \sum_{g' \subset g} N(g', g) \kappa(g'), \tag{A6}$$

where $N(g', g)$ is the number of subclusters of a cluster in g which belong to the class g'.

Typically, the clusters c are represented by graphs, where vertices represent the sites and edges represent the bonds. Here, we have bonds which contain more than two sites, so one can analogously represent clusters by hypergraphs. Essentially, we use the König representation [26,27] of the corresponding hypergraphs to represent the clusters by bipartite graphs [17]. Two clusters represented by isomorphic graphs are structurally equivalent or isomorphic. Next, the product states involved in a matrix element can be incorporated using additional vertex colors within the graphs. The equivalence of clusters then corresponds to the (color-preserving) isomorphism of the respective graphs with the additional vertex colors [17].

Typically, $K(g)$ is evaluated perturbatively on a representative cluster of the class g [15,16]. In a perturbative calculation it is possible to replace the explicit subtraction of reduced contributions from proper subclusters in order to obtain $\kappa(g)$ by a bookkeeping technique [28]. This technique ensures that only the perturbative processes which act on all bonds of the representative cluster are taken into account for $\kappa(g)$. This also implies that a cluster with k bonds can only contribute in perturbation order k or higher. Accordingly, for an order-k perturbative expansion, it suffices to consider clusters up to k bonds to obtain the series expansion for $K(C)$.

For the calculation of the ground-state energy we either determine the expectation value of the effective Hamiltonian with respect to the unperturbed ground state or we apply matrix perturbation theory. In this case it is obvious that the ground-state energies on structurally equivalent clusters agree [15]. In order to derive hopping elements $t_{i,j}$ we subtract the ground-state energy E_0 from the effective Hamiltonian H_{eff} as suggested by Gelfand [23] and calculate the matrix elements with respect to the product states, where one excitation is at site i or j, respectively,

$$t_{i,j} = \langle j | H_{\mathrm{eff}} - E_0 | i \rangle. \tag{A7}$$

Importantly, to evaluate $t_{i,j}$ on a cluster c one subtracts the ground-state energy $E_0(c)$ of the cluster c from the effective Hamiltonian on c. As a consequence, the reduced contribution of any cluster which does not contain the sites i and j vanishes. As the Hamiltonian on two structurally equivalent clusters is the same up to a renumbering of the sites, their contributions agree if they correspond to equivalent matrix elements of

$H_{\text{eff}} - E_0$ on the clusters. This also generalizes to hopping elements of n particles

$$t_{i_1,\dots,i_n,j_1,\dots,j_n} = \langle j_1,\dots,j_n|H_{\text{eff}} - E_0|i_1,\dots,i_n\rangle. \quad \text{(A8)}$$

Here, the clusters with nonvanishing reduced contribution need to contain at least one of the sites which are occupied in the initial state and all sites which change their local state [17]. From these hopping elements one can obtain the irreducible hopping elements by appropriately subtracting the lower particle hopping elements [20]. While for the ground-state energy only linked clusters have a nonvanishing reduced contribution, this does not necessarily hold in the case of hopping elements. Indeed, some methods assign nonvanishing reduced contributions to disconnected clusters [16]. For a cluster-additive effective Hamiltonian the reduced contributions of disconnected clusters vanish [29]. The effective Hamiltonian obtained by the pCUT method [19,20] is guaranteed to be cluster additive as long as the unperturbed Hamiltonian is cluster additive [30,31]. Alternatively, one can deduce that the contributions of the effective Hamiltonian from pCUT vanish on disconnected clusters by showing that it can be written as a perturbative commutator expansion [32].

For the ground-state energy we also evaluate the reduced contributions of the clusters using exact diagonalization and subtracting the reduced contributions of proper subclusters. Evaluating the contributions of the clusters with exact diagonalization within a linked-cluster expansion has been dubbed exact linked cluster expansion (ELCE) [33,34] or numerical linked cluster expansion (NLCE) [18]. For a short introduction to NLCE see also Ref. [35]. These expansions are typically done for extensive quantities like the ground-state energy. However, it is possible to derive nonperturbative results for higher particle sectors as well [29,34,36].

In our case we obtain the ground-state energy of a cluster from the matrix representing $\mathcal{H}_{\text{qNM}}$ on the given cluster in the sector of the fully polarized state corresponding to the ground state at $J = 0$. The basis for this matrix can be obtained by repeatedly acting with the coupling term on this state until no new basis states are generated. Then, we calculate the matrix elements in this basis and determine the lowest eigenvalue of the resulting matrix with the Lanczos method [37–39].

In a perturbative calculation one takes into account any class of connected subclusters which can possibly contribute in the desired perturbation order to obtain the perturbative series in the thermodynamic limit. In NLCE the truncation is done in the choice and size of the clusters and hence is nonperturbative [34]. Physically, the size of the considered clusters determines the spatial extent of quantum fluctuations treated within an NLCE calculation. Actually, schemes based on different choices of clusters can lead to improved results [40–42].

In summary, in this work we apply the procedure described in Ref. [17] in order to calculate the matrix elements of the effective Hamiltonian. First, we generate all relevant subclusters for a given hopping element or the ground-state energy. During this procedure we sort the subclusters into appropriate equivalence classes and keep track of the embedding factors. Afterwards, we evaluate the reduced contributions of these classes. Finally, we sum up the properly weighed contributions in order to obtain the desired result.

APPENDIX B: BARE SERIES OF GROUND-STATE ENERGY AND EXCITATION GAPS

The series for the ground-state energy per site in units of $\Gamma = \frac{1}{2}$ is calculated up to order 26 and reads

$$
\begin{aligned}
\frac{E_0}{N} = &-\frac{1}{2} - \frac{1}{3}J^2 - \frac{2}{27}J^4 - \frac{694}{8505}J^6 - \frac{87\,917}{714\,420}J^8 - \frac{1\,163\,156\,201}{5\,063\,451\,750}J^{10} - \frac{37\,554\,176\,289\,949}{76\,559\,390\,460\,000}J^{12} \\
&- \frac{11\,683\,996\,058\,218\,949\,671}{10\,345\,853\,229\,812\,100\,000}J^{14} - \frac{61\,969\,629\,185\,820\,865\,703\,757\,811}{22\,369\,390\,019\,370\,530\,136\,000\,000}J^{16} \\
&- \frac{366\,126\,366\,318\,767\,391\,658\,088\,809\,316\,147}{51\,389\,087\,844\,549\,822\,028\,782\,120\,000\,000}J^{18} \\
&- \frac{7\,180\,291\,157\,644\,353\,011\,347\,796\,827\,422\,626\,494\,913}{377\,778\,862\,591\,504\,266\,872\,355\,265\,169\,280\,000\,000}J^{20} \\
&- \frac{344\,371\,159\,846\,708\,207\,005\,245\,975\,888\,183\,886\,739\,063\,098\,907}{6\,595\,808\,140\,242\,338\,440\,210\,408\,155\,617\,664\,341\,760\,000\,000}J^{22} \\
&- \frac{8\,458\,783\,982\,889\,010\,392\,413\,115\,078\,905\,896\,242\,564\,195\,637\,263\,595\,308\,619}{57\,579\,564\,833\,844\,486\,970\,612\,044\,494\,666\,792\,375\,213\,448\,960\,000\,000\,000}J^{24} \\
&- \frac{6\,094\,307\,456\,345\,282\,285\,613\,515\,218\,215\,816\,652\,048\,109\,273\,373\,916\,121\,215\,182\,638\,251}{14\,451\,289\,168\,650\,119\,698\,445\,377\,495\,743\,278\,705\,265\,545\,839\,970\,529\,600\,000\,000\,000}J^{26}. \quad \text{(B1)}
\end{aligned}
$$

Since the 1QP configuration is completely immobile, the block in the effective Hamiltonian is one-dimensional and the series obtained up to order 14 in units of $\Gamma = \frac{1}{2}$ reads

$$
\begin{aligned}
\Delta_1 = &1 - 2J^2 + \frac{10}{9}J^4 - \frac{398}{45}J^6 + \frac{21\,286\,241}{893\,025}J^8 - \frac{34\,989\,373\,088}{281\,302\,875}J^{10} \\
&+ \frac{2\,125\,889\,739\,834\,149}{4\,253\,299\,470\,000}J^{12} - \frac{683\,607\,613\,238\,271\,693\,151}{265\,278\,287\,943\,900\,000}J^{14}. \quad \text{(B2)}
\end{aligned}
$$

The mobility of all 2QP configurations is highly restricted and the corresponding block in the effective Hamiltonian is of finite size. In order 12 perturbation theory, the block is of size 15×15, therefore yielding 15 energy eigenvalues. The 2QP energy eigenvalue decreasing strongest in leading order and therefore considered as the 2QP gap reads, in units of $\Gamma = \frac{1}{2}$,

$$\Delta_2 = 2 - 8J^2 + \frac{1336}{27}J^4 - \frac{6\,264\,848}{8505}J^6 + \frac{427\,973\,156}{33\,075}J^8 - \frac{2\,595\,333\,024\,547\,577}{10\,126\,903\,500}J^{10} + \frac{1\,543\,912\,949\,140\,866\,037}{283\,553\,298\,000}J^{12}.$$
(B3)

The series for the first eigenvalue of the 3QP sector in units of $\Gamma = \frac{1}{2}$ for $\mathbf{k} = 0$ up to order 12 reads

$$\Delta_3^{(1)} = 3 - \frac{2}{3}(10 + \sqrt{82})J^2 + \frac{(109\,054 + 12\,907\sqrt{82})}{27(82 + \sqrt{82})}J^4 - \frac{4(1\,436\,807\,939\,437 + 154\,950\,111\,676\sqrt{82})}{8505(82 + \sqrt{82})^3}J^6$$

$$+ \frac{(346\,835\,035\,620\,091\,968\,700 + 38\,457\,664\,526\,290\,637\,983\sqrt{82})}{2\,679\,075(82 + \sqrt{82})^5}J^8$$

$$- \frac{(143\,882\,555\,062\,725\,026\,268\,280\,765\,837 + 15\,878\,921\,718\,665\,450\,600\,555\,048\,341\sqrt{82})}{5\,063\,451\,750(82 + \sqrt{82})^7}J^{10}$$

$$+ \left(\frac{63\,875\,776\,145\,970\,660\,095\,856\,118\,712\,991\,441\,467}{9\,569\,923\,807\,500(82 + \sqrt{82})^9} \right.$$

$$\left. + \frac{7\,054\,556\,156\,002\,646\,215\,050\,241\,827\,786\,693\,722\sqrt{82}}{9\,569\,923\,807\,500(82 + \sqrt{82})^9} \right)J^{12}.$$
(B4)

The series for the second eigenvalue of the 3QP sector in units of $\Gamma = \frac{1}{2}$ for $\mathbf{k} = 0$ up to order 12 reads

$$\Delta_3^{(2)} = 3 - 6J^2 + \frac{10}{3}J^4 - \frac{398}{15}J^6 + \frac{20\,510\,669}{297\,675}J^8 - \frac{170\,229\,112\,967}{337\,563\,450}J^{10} + \frac{117\,051\,872\,376\,412\,993}{22\,967\,817\,138\,000}J^{12}.$$
(B5)

The series for the third eigenvalue of the 3QP sector in units of $\Gamma = \frac{1}{2}$ for $\mathbf{k} = 0$ up to order 12 reads

$$\Delta_3^{(3)} = 3 + \frac{2}{3}(-10 + \sqrt{82})J^2 + \frac{(-109\,054 + 12\,907\sqrt{82})}{27(-82 + \sqrt{82})}J^4 - \frac{4(-1\,436\,807\,939\,437 + 154\,950\,111\,676\sqrt{82})}{8505(-82 + \sqrt{82})^3}J^6$$

$$+ \frac{(-346\,835\,035\,620\,091\,968\,700 + 38\,457\,664\,526\,290\,637\,983\sqrt{82})}{2\,679\,075(-82 + \sqrt{82})^5}J^8$$

$$- \frac{(-143\,882\,555\,062\,725\,026\,268\,280\,765\,837 + 15\,878\,921\,718\,665\,450\,600\,555\,048\,341\sqrt{82})}{5\,063\,451\,750(-82 + \sqrt{82})^7}J^{10}$$

$$+ \left(\frac{-63\,875\,776\,145\,970\,660\,095\,856\,118\,712\,991\,441\,467}{9\,569\,923\,807\,500(-82 + \sqrt{82})^9} \right.$$

$$\left. + \frac{7\,054\,556\,156\,002\,646\,215\,050\,241\,827\,786\,693\,722\sqrt{82}}{9\,569\,923\,807\,500(-82 + \sqrt{82})^9} \right)J^{12}.$$
(B6)

APPENDIX C: DLOG PADÉ EXTRAPOLATIONS

To extract the quantum-critical point including critical exponents from the pCUT method well beyond the radius of convergence of the pure high-order series, we use Dlog Padé extrapolations. For a detailed description of Dlog Padés and its application to critical phenomena we refer to Refs. [43,44]. The Padé extrapolant of a physical quantity κ given as a perturbative series is defined as

$$P[L, M]_\kappa = \frac{P_L(\lambda)}{Q_M(\lambda)} = \frac{p_0 + p_1\lambda + \cdots + p_L\lambda^L}{1 + q_1\lambda + \cdots + q_M\lambda^M}$$
(C1)

with $p_i, q_i \in \mathbb{R}$ and the degrees L, M of $P_L(x)$ and $Q_M(x)$ with $r \equiv L + M$, i.e., the Taylor expansion of Eq. (C1) about $\lambda = 0$

up to order r must recover the quantity κ up to the same order. For Dlog Padé extrapolants we introduce

$$\mathcal{D}(\lambda) = \frac{d}{d\lambda} \ln(\kappa) \equiv P[L, M]_\mathcal{D},$$
(C2)

the Padé extrapolant of the logarithmic derivative $\mathcal{D}$ with $r - 1 = L + M$. Thus, the Dlog Padé extrapolant of κ is given by

$$dP[L, M]_\kappa = \exp\left(\int_0^\lambda P[L, M]_\mathcal{D} \, d\lambda' \right).$$
(C3)

Given a dominant power-law behavior $\kappa \sim |\lambda - \lambda_c|^{-\theta}$, an estimate for the critical point λ_c can be determined by excluding spurious extrapolants and analyzing the physical pole of

$P[L, M]_{\mathcal{D}}$. If λ_c is known, we can define biased Dlog Padés by the Padé extrapolant

$$\theta^* = (\lambda_c - \lambda)\frac{d}{d\lambda}\ln(\kappa) \equiv P[L, M]_{\theta^*}. \qquad (C4)$$

In the unbiased as well as the biased case we can extract estimates for the critical exponent θ by calculating the residua

$$\theta_{\text{unbiased}} = \text{Res}\, P[L, M]_{\mathcal{D}}|_{\lambda=\lambda_c},$$
$$\theta_{\text{biased}} = \text{Res}\, P[L, M]_{\theta^*}|_{\lambda=\lambda_c}. \qquad (C5)$$

[1] R. M. Nandkishore and M. Hermele, Fractons, Annu. Rev. Condens. Matter Phys. **10**, 295 (2019).

[2] S. Bravyi and J. Haah, Quantum self-correction in the 3D cubic code model, Phys. Rev. Lett. **111**, 200501 (2013).

[3] B. Yoshida, Exotic topological order in fractal spin liquids, Phys. Rev. B **88**, 125122 (2013).

[4] G. B. Halász, T. H. Hsieh, and L. Balents, Fracton topological phases from strongly coupled spin chains, Phys. Rev. Lett. **119**, 257202 (2017).

[5] S. Pai and M. Hermele, Fracton fusion and statistics, Phys. Rev. B **100**, 195136 (2019).

[6] W. Shirley, K. Slagle, and X. Chen, Twisted foliated fracton phases, Phys. Rev. B **102**, 115103 (2020).

[7] S. Vijay, J. Haah, and L. Fu, Fracton topological order, generalized lattice gauge theory, and duality, Phys. Rev. B **94**, 235157 (2016).

[8] J. Haah, Local stabilizer codes in three dimensions without string logical operators, Phys. Rev. A **83**, 042330 (2011).

[9] T. Devakul, S. A. Parameswaran, and S. L. Sondhi, Correlation function diagnostics for type-I fracton phases, Phys. Rev. B **97**, 041110(R) (2018).

[10] M. Mühlhauser, M. R. Walther, D. A. Reiss, and K. P. Schmidt, Quantum robustness of fracton phases, Phys. Rev. B **101**, 054426 (2020).

[11] M. Mühlhauser, K. P. Schmidt, J. Vidal, and M. R. Walther, Competing topological orders in three dimensions, SciPost Phys. **12**, 069 (2022).

[12] M. E. J. Newman and C. Moore, Glassy dynamics and aging in an exactly solvable spin model, Phys. Rev. E **60**, 5068 (1999).

[13] Z. Zhou, X.-F. Zhang, F. Pollmann, and Y. You, Fractal quantum phase transitions: Critical phenomena beyond renormalization, arXiv:2105.05851.

[14] L. M. Vasiloiu, T. H. E. Oakes, F. Carollo, and J. P. Garrahan, Trajectory phase transitions in noninteracting spin systems, Phys. Rev. E **101**, 042115 (2020).

[15] M. P. Gelfand and R. R. P. Singh, High-order convergent expansions for quantum many particle systems, Adv. Phys. **49**, 93 (2000).

[16] J. Oitmaa, C. Hamer, and W. Zheng, *Series Expansion Methods for Strongly Interacting Lattice Models* (Cambridge University Press, Cambridge, 2006).

[17] M. Mühlhauser and K. P. Schmidt, Linked cluster expansions via hypergraph decompositions, Phys. Rev. E **105**, 064110 (2022).

[18] M. Rigol, T. Bryant, and R. R. P. Singh, Numerical linked-cluster approach to quantum lattice models, Phys. Rev. Lett. **97**, 187202 (2006).

[19] C. Knetter and G. S. Uhrig, Perturbation theory by flow equations: Dimerized and frustrated S = 1/2 chain, Eur. Phys. J. B **13**, 209 (2000).

[20] C. Knetter, K. P. Schmidt, and G. S. Uhrig, The structure of operators in effective particle-conserving models, J. Phys. A: Math. Gen. **36**, 7889 (2003).

[21] K. Sfairopoulos, L. Causer, J. F. Mair, and J. P. Garrahan, Boundary conditions dependence of the phase transition in the quantum Newman-Moore model, arXiv:2301.02826.

[22] N. E. Myerson-Jain, S. Yan, D. Weld, and C. Xu, Construction of fractal order and phase transition with Rydberg atoms, Phys. Rev. Lett. **128**, 017601 (2022).

[23] M. P. Gelfand, Series expansions for excited states of quantum lattice models, Solid State Commun. **98**, 11 (1996).

[24] S. Trebst, H. Monien, C. J. Hamer, Z. Weihong, and R. R. P. Singh, Strong-coupling expansions for multiparticle excitations: Continuum and bound states, Phys. Rev. Lett. **85**, 4373 (2000).

[25] W. Zheng, C. J. Hamer, R. R. P. Singh, S. Trebst, and H. Monien, Linked cluster series expansions for two-particle bound states, Phys. Rev. B **63**, 144410 (2001).

[26] A. A. Zykov, HYPERGRAPHS, Russ. Math. Surv. **29**, 89 (1974).

[27] E. V. Konstantinova and V. A. Skorobogatov, Molecular hypergraphs: The new representation of nonclassical molecular structures with polycentric delocalized bonds, J. Chem. Inf. Comput. Sci. **35**, 472 (1995).

[28] K. Coester and K. P. Schmidt, Optimizing linked-cluster expansions by white graphs, Phys. Rev. E **92**, 022118 (2015).

[29] M. Hörmann and K. P. Schmidt, Projective cluster-additive transformation for quantum lattice models, SciPost Phys. **15**, 097 (2023).

[30] M. D. Schulz, Topological phase transitions driven by non-Abelian anyons, Ph.D. thesis, Technische Universität Dortmund, 2014.

[31] K. Cöster, Quasiparticle pictures and graphs - from perturbative to non-perturbative linked-cluster expansions, Ph.D. thesis, Technische Universität Dortmund, 2015.

[32] S. Dusuel, M. Kamfor, K. P. Schmidt, R. Thomale, and J. Vidal, Bound states in two-dimensional spin systems near the Ising limit: A quantum finite-lattice study, Phys. Rev. B **81**, 064412 (2010).

[33] A. Irving and C. Hamer, Methods in Hamiltonian lattice field theory (II). Linked-cluster expansions, Nucl. Phys. B **230**, 361 (1984).

[34] C. J. Hamer and A. C. Irving, Cluster expansions in the (2+1)D ising model, J. Phys. A: Math. Gen. **17**, 1649 (1984).

[35] B. Tang, E. Khatami, and M. Rigol, A short introduction to numerical linked-cluster expansions, Comput. Phys. Commun. **184**, 557 (2013).

[36] H. Y. Yang and K. P. Schmidt, Effective models for gapped phases of strongly correlated quantum lattice models, Europhys. Lett. **94**, 17004 (2011).

[37] C. Lanczos, An iteration method for the solution of the eigenvalue problem of linear differential and integral operators, J. Res. Natl. Bur. Stand. **45**, 255 (1950).

[38] C. C. Paige, Accuracy and effectiveness of the Lanczos algorithm for the symmetric eigenproblem, Linear Algebra and its Applications **34**, 235 (1980).

[39] A. W. Sandvik, Computational studies of quantum spin systems AIP Conf. Proc. **1297**, 135 (2010).

[40] M. Rigol, T. Bryant, and R. R. P. Singh, Numerical linked-cluster algorithms. I. Spin systems on square, triangular, and kagomé lattices, Phys. Rev. E **75**, 061118 (2007).

[41] D. Ixert and K. P. Schmidt, Nonperturbative linked-cluster expansions in long-range ordered quantum systems, Phys. Rev. B **94**, 195133 (2016).

[42] R. Schäfer, I. Hagymási, R. Moessner, and D. J. Luitz, Pyrochlore $s = \frac{1}{2}$ Heisenberg antiferromagnet at finite temperature, Phys. Rev. B **102**, 054408 (2020).

[43] G. Baker, *Essentials of Padé Approximants* (Elsevier Science, New York, 1975).

[44] A. J. Guttmann, Asymptotic analysis of power-series expansions, in *Phase Transitions and Critical Phenomena*, edited by C. Domb and J. L. Lebowitz (Academic Press, New York, 1989), Vol. 13.